Available online at www.sciencedirect.com
ScienceDirect
Trans. Nonferrous Met. Soc. China 32(2022) 2541−2556
Transactions of Nonferrous Metals Society of China
www.tnmsc.cn

Hot shear deformation constitutive analysis of fine-grained ZK60 Mg alloy sheet fabricated via dual equal channel lateral extrusion and sheet extrusion

N. FAKHAR[1], M. SABBAGHIAN[2]

1. Mechanical Engineering Department, Hamedan University of Technology, Hamedan, Iran;
2. School of Metallurgical and Materials Engineering, College of Engineering, University of Tehran, Tehran, Iran

Received 27 July 2021; accepted 1 April 2022

Abstract: Dual equal channel lateral extrusion (DECLE) process with various passes followed by sheet extrusion process was performed to produce fine-grained ZK60 alloy sheets. The coarse grain structure of the annealed sample after applying sheet extrusion (size: 68 μm) changed to fine grains of 6.0 and 5.2 μm after 3 and 5 passes of DECLE and following extrusion. The hot shear deformation behavior of samples was studied by developing constitutive equations based on shear punch test (SPT) results. SPT was carried out in the temperature range of 200−300 °C and strain rate range of 0.003−0.33 s^{-1}. The activation energy of 125−139 kJ/mol and the stress exponent of 3.5−4.2 were calculated for all conditions, which indicated that dislocation creep, controlled by dislocation climb and solute drag mechanism, acted as the main hot deformation mechanism. It was concluded that material constants of n and Q are dependent on the microstructural factors such as grain size and second phase particle fraction, and the relationship of which was anticipated using a 3D surface curve. Moreover, the similar strong basal texture of extruded sheets gave rise to the same deformation mechanisms during SPT and similar n and Q values for ZK60 alloy.
Key words: ZK60 Mg alloy; constitutive equation; extrusion; hot deformation; shear punch test; metal forming

1 Introduction

Magnesium alloys have low density (1.7−2.0 g/cm^3), good castability, machinability, and high specific strength that make them promising candidates to develop structural parts to be used in automotive and aerospace industries [1] . The main challenge for expanding use of Mg alloys is their low formability, especially in the wrought condition at room temperature that is caused by the limited number of slip systems in the hexagonal close-packed (HCP) crystal structure [1]. Several approaches such as deformation at elevated temperatures [2], using alloying elements [3] and grain refinement by the thermomechanical processes [4−6] are considered to enhance the formability of the Mg alloys.

In Mg alloys, low-temperature deformation depends on slip on basal systems [7]. To activate non-basal slip planes such as pyramidal and prismatic planes, the temperature could be increased [8]. Besides, grain boundary sliding (GBS), as one of the effective deformation mechanisms activated in the fine-grained (FG) Mg alloys, could be obtained generally at high temperatures [9]. On the other hand, texture weakening occurs during the hot deformation of Mg alloys and improves the formability of the processed parts [8]. To refine the microstructure of Mg alloys and consequently facilitate some mechanisms such as GBS, severe plastic deformation (SPD) techniques like equal channel angular pressing (ECAP) [10] attracted significant

Corresponding author: N. FAKHAR, E-mail: n.fakhar@hut.ac.ir, naemeh.fakhar@gmail.com
DOI: 10.1016/S1003-6326(22)65964-8

attention recently in comparison to other traditional processes, such as extrusion. By conducting these processes, grain size would be reduced, and second phase particles' state (size, shape, distribution, and even volume fraction) would be altered [4,11]. As another achievement, the texture component will evolve after the SPD process [12,13].

An SPD method known as dual equal channel lateral extrusion (DECLE) that is suitable for grain refinement of thick samples, has been recently introduced to produce a fine grain microstructure in magnesium alloys [14]. In this technique, a rectangular cube is severely deformed into a closed T-shaped die, such as a couple of back-to-back 90° ECAP procedure [15]. The main privilege of the DECLE method compared with the ECAP is performing a larger effective strain (~1.4) through each pass. FERESHTEH-SANIEE et al [16] have shown that the sheet extrusion process can be performed on the DECLEed plates and FG Mg sheet with enhanced strength, and desirable ductility could be produced [9]. Hence, these modified Mg sheet alloys are suitable candidates for sheet forming processes to fabricate different industrial parts.

To develop a sound and defect-free wrought Mg sheet part for utilizing in automotive or aerospace industries, it is necessary to investigate the alloy flow stress behavior at elevated temperatures. To assess such behavior, researchers usually use compression test [17,18], sometimes tensile testing methods [19] at various temperatures and strain rates, and drive constitutive equations to predict the flow procedure under other deformation conditions. Recently, the shear punch test (SPT) has been introduced as a suitable miniature method to assess mechanical properties such as shear yield stress (SYS) and ultimate shear strength (USS) of both cast and wrought alloys at room and high temperatures [4,11,20]. In this test, a flat-ended cylindrical punch is driven through a securely clamped sheet sample, punching a circular disk from it [21]. SPT was used to investigate the hot deformation behavior of different Mg alloys such as Mg−Gd alloys [22,23], and it was suggested that the developed constitutive relations are completely reasonable.

ZK60, as one of the most commercial Mg alloys, has attracted numerous attentions [24,25]. Several researchers investigated hot deformation behavior of this alloy under wrought condition, the summary of which is present in Table 1. In these researches, different concepts such as the derivation of some constitutive equations to predict flow behavior, and evaluation of the influences of texture or addition of alloying elements on the properties of ZK60 alloy were considered. On the other hand, the investigation of the hot deformation behavior of ZK60 alloy after processing via SPD techniques is scant. Besides, to the best of the author's knowledge, SPT has not yet been used for estimating the hot shear deformation behavior of ZK60 alloy thin sheets by constitutive analysis. In this work, the hot shear behavior of ZK60 alloy sheet processed by a combination of DECLE as an SPD method and consequently sheet extrusion was

Table 1 Literature review on hot deformation behavior of ZK60 alloy

Processing route	Testing method	Temperature/°C	Strain rate/s^{-1}	Main objective	Ref.
Extruded	Compression	300−450	1×10^{-3}–1	Effect of direction on flow behavior and DRX	[1]
Rolled sheet	Tensile	100−300	6×10^{-4}	Effect of texture weakening on strength anisotropy	[8]
Extruded	Compression	250−450	1×10^{-3}–10	Driving constitutive equation and processing maps	[26]
ECAPed	Tensile	200, 225	3.3×10^{-5}–1×10^{-2}	Superplastic behavior	[27]
Extruded	Compression	250−400	1×10^{-3}–1	Driving constitutive equation and processing maps	[28]
ECAPed	Tensile	200−250	1.67×10^{-3}	Superplastic behavior	[29]
Cast + Homogenized extruded	Compression	300−450	1×10^{-3}–1	Driving constitutive equation	[30]
Extruded plate	Compression	200−500	3×10^{-4}–10	Effect of sample direction on flow behavior; Driving processing maps	[31]

modeled by using the Arrhenius equation. To achieve the material constants of the equation, shear punch test results at high temperatures were obtained.

2 Experimental

Cast ZK60 Mg alloy with a composition of 6 wt.% Zn, 0.6 wt% Zr, and remained Mg was prepared in the form of 20 mm-thick billets. To enhance the homogeneity of the as-cast structure, the billets were annealed at 400 °C for 12 h. Hot-rolling was performed to reduce the thickness of each plate to 10 mm before conducting DECLE. Afterward, the plates were machined to 50 mm × 50 mm × 10 mm specimens for the DECLE process. Prepared samples for DECLE were annealed at 400 °C for 1 h (hereafter called the annealed sample).

The DECLE experiments were performed using a hydraulic press with a constant ram velocity of 1 mm/min. To reduce the friction in hot compression, MoS_2 was used as the lubricant. To heat the die-set and billets, several heating elements were located in the die. The temperature during the process was controlled using a thermocouple. All the DECLE experiments were performed at 250 °C and through Route B [9]. The DECLE process was conducted up to 5 passes. To produce ZK60 Mg sheets, the sheet extrusion process was carried out with the 1-, 3-, and 5-pass DECLEed samples. All the sheet extrusion experiments were conducted at 220 °C using an extrusion speed of 0.3 mm/min and ZK60 sheets were produced with a thickness of 1.3 mm. Figure 1 exhibits the schematic illustration of the processes used to fabricate ZK60 sheets. Hereafter, the sheet extruded from the annealed material was denoted as AE, from the 1-passed DECLE process as A1DE, from the 3-passed DECLE process as A3DE, and finally from the 5-passed DECLE process as A5DE. These abbreviations specify the processing histories of each sample and are explained more in Table 2.

To reveal the microstructure of processed samples, Union Versamet optical microscope (OM) and a Qunta 450 scanning electron microscope (SEM) were used. Before the microstructural observations, the samples were polished and consequently etched by an acetic picral solution. The second phase particles were analyzed by energy dispersive spectroscopy (EDS).

To assess the hot shear deformation behavior of the ZK60 sheets, SPT was used. The samples prepared for SPT had a dimension of 10 mm × 10 mm × 1.3 mm. The sampling position for SPT is demonstrated in Fig. 1. By polishing both sides of the sheet, the thickness of SPT specimens was reduced to about 0.7 mm with a tolerance of ±0.05. SPT was carried out using a 50 kN universal testing machine equipped with a chamber furnace. A temperature range of 200−300 °C and a shear strain rate range of 0.003−0.33 s^{-1} were selected for SPT

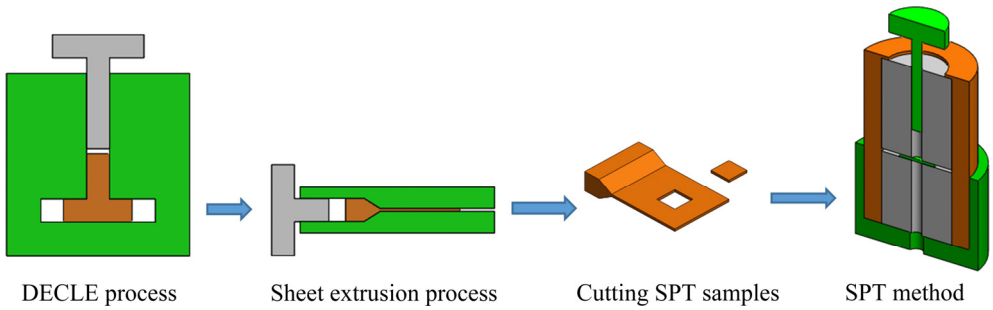

Fig. 1 Scheme of investigated material forming and sampling method for shear punch testing

Table 2 Processing histories of ZK60 sheets and notations

Notation	Processing route
AE	Hot rolled + annealed at 400 °C + sheet extrusion at 220 °C
A1DE	Hot rolled + annealed at 400 °C + 1-pass DECLE at 250 °C + sheet extrusion at 220 °C
A3DE	Hot rolled + annealed at 400 °C + 3-pass DECLE at 250 °C + sheet extrusion at 220 °C
A5DE	Hot rolled + annealed at 400 °C + 5-pass DECLE at 250 °C + sheet extrusion at 220 °C

experiments. Every SPT was conducted twice to ensure the repeatability of the results. The following equations were used to calculate the shear stress (τ) and shear strain rate ($\dot{\gamma}$) from the load−displacement data obtained via SPT:

$$\tau = \frac{P}{\pi dt} \tag{1}$$

$$\dot{\gamma} = \frac{1}{2}\left(\frac{\dot{z}}{W}\right) \tag{2}$$

where P is the punch load, d is the average value of the punch and die diameters, t is the specimen thickness, $\dot{z}$ is the punch speed, and W is the punch−die clearance. The SPT results were plotted as the shear stress versus normalized displacement curves. The normalized displacement values are defined as the ratio of the shear punch displacement to the sample thickness.

3 Results and discussion

3.1 Microstructure

Since the microstructure of the ZK60 alloy sheets depends on the initial microstructure before extrusion, Fig. 2 reveals OM images of the ZK60 alloy for annealed and the DECLE processed samples. A coarse grain structure (average grain size ~68 μm) was obtained after hot rolling (Fig. 2(a)). This type of microstructure has been reported previously in hot rolled Mg alloys [2]. It can be inferred from Figs. 2(b−d) that straining via 1, 3, and 5 passes of the DECLE process leads to gradual grain refinement in the ZK60 alloy, which can be attributed to the dynamic recrystallization (DRX) phenomenon [25]. It is evident that in the 1-pass processed sample a bimodal microstructure known as the necklace structure including fine DRXed grains (average grain size ~2 μm) around coarse un-DRXed grains (grain size 20−80 μm) was developed that is indicative of the partial DRX [32]. Partial DRX can be a sign of insufficient applied strain (about 1.4) through the first pass of DECLE. Similar results were observed for ZK60 alloy deformed by other SPD techniques such as 1 pass of MDF [13], and 1 and 2 passes of ECAP [33]. These results could be explained by the limited number of slip systems in Mg alloys, which means that the number of grains having favorable orientations for DRX was small during the first pass of the SPD process. Further deformation by 3 and 5

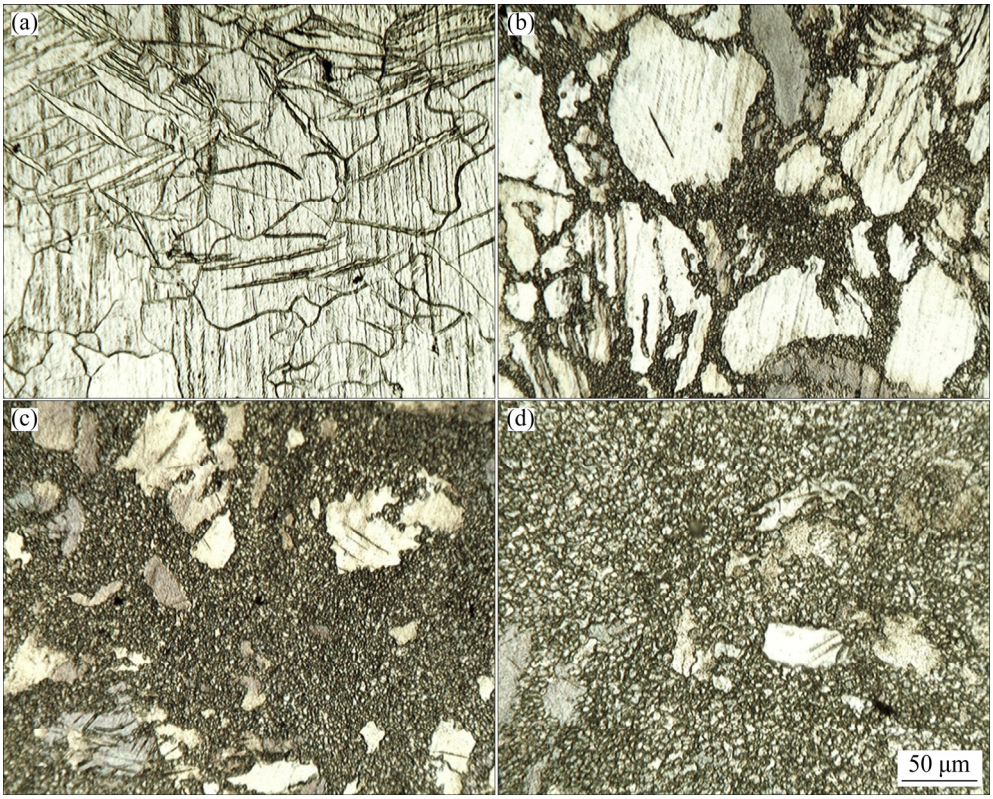

Fig. 2 Optical images of annealed (a), 1-pass DECLEed (b), 3-pass DECLEed (c), and 5-pass DECLEed (d) samples

passes of DECLE resulted in a more uniform grain structure with smaller average grain size and decreased volume fraction of coarse-grained regions. It is in agreement with the results reported for ZK60 alloy fabricated by other SPD procedures such as ECAP [34]. A more detailed analysis of second phase particles and texture evolution can be found in our previous research [25].

The OM and SEM images of extruded sheets of ZK60 alloy are exhibited in Figs. 3−5. Performing the extrusion process at 220 °C on the annealed and DECLE processed samples resulted in more grain refinement via DRX. However, the microstructure of the AE sample still comprises large elongated un-DRXed grains along extrusion direction (ED), and the volume fraction of fine-grain regions was significantly increased in comparison to the initial microstructure of annealed sample. The average grain size of fine regions was determined as 2.8 μm, and the length of elongated grains (with an aspect ratio greater than 2) was in the range of 150−350 μm. Contrary to the AE sample, extrusion completely modified the microstructure of DECLE samples, and a relatively homogeneous fine grain structure with an average grain size of 7.1, 6.0, and 5.2 μm was produced in A1DE, A3DE, and A5DE specimens, respectively.

During DRX, the processes of nucleation and

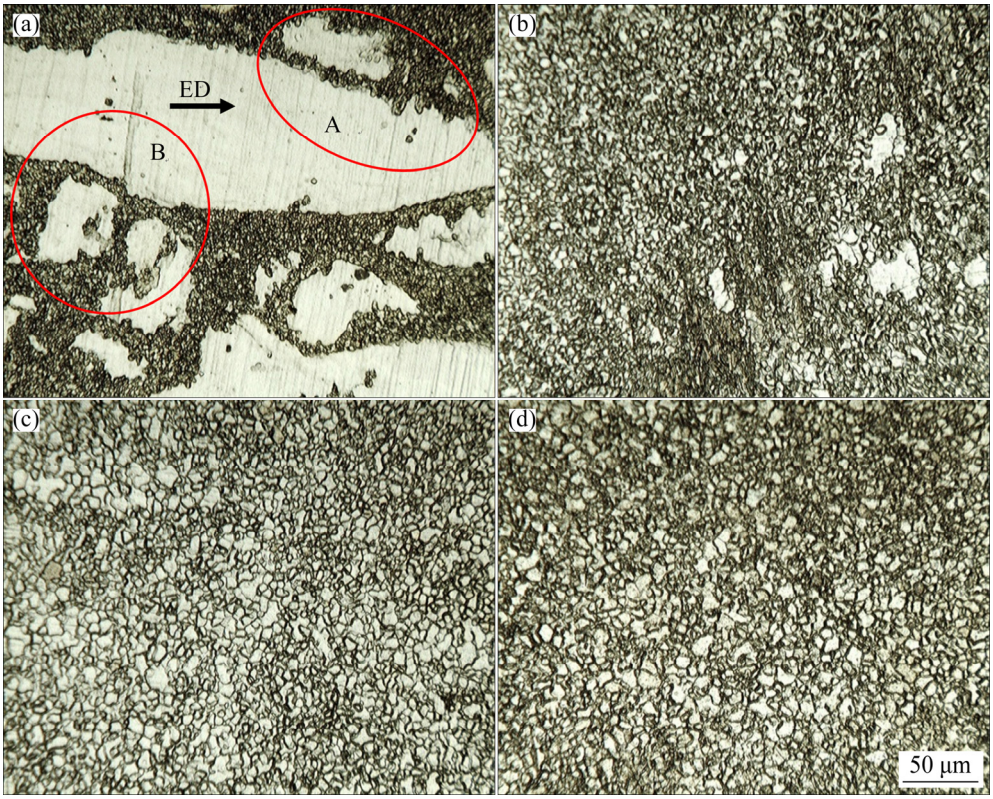

Fig. 3 Optical images of AE (a), A1DE (b), A3DE (c), and A5DE (d) samples

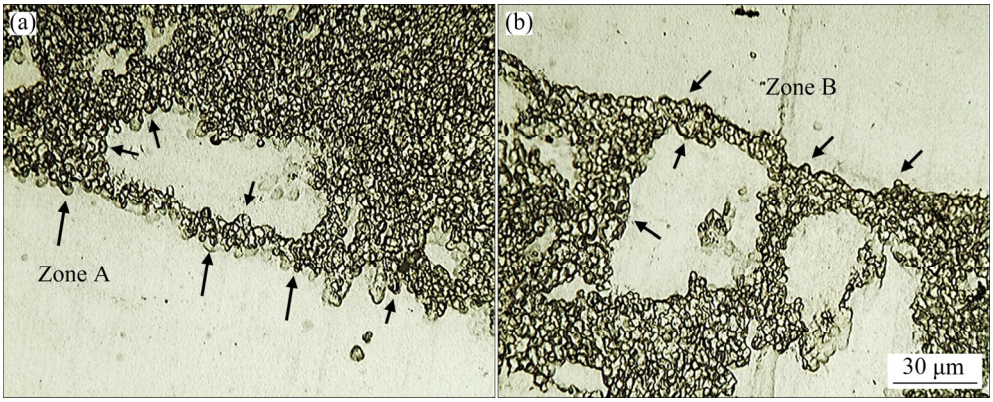

Fig. 4 High-magnification micrographs of regions marked by red ellipses in Fig. 3(a): (a) Zone A; (b) Zone B

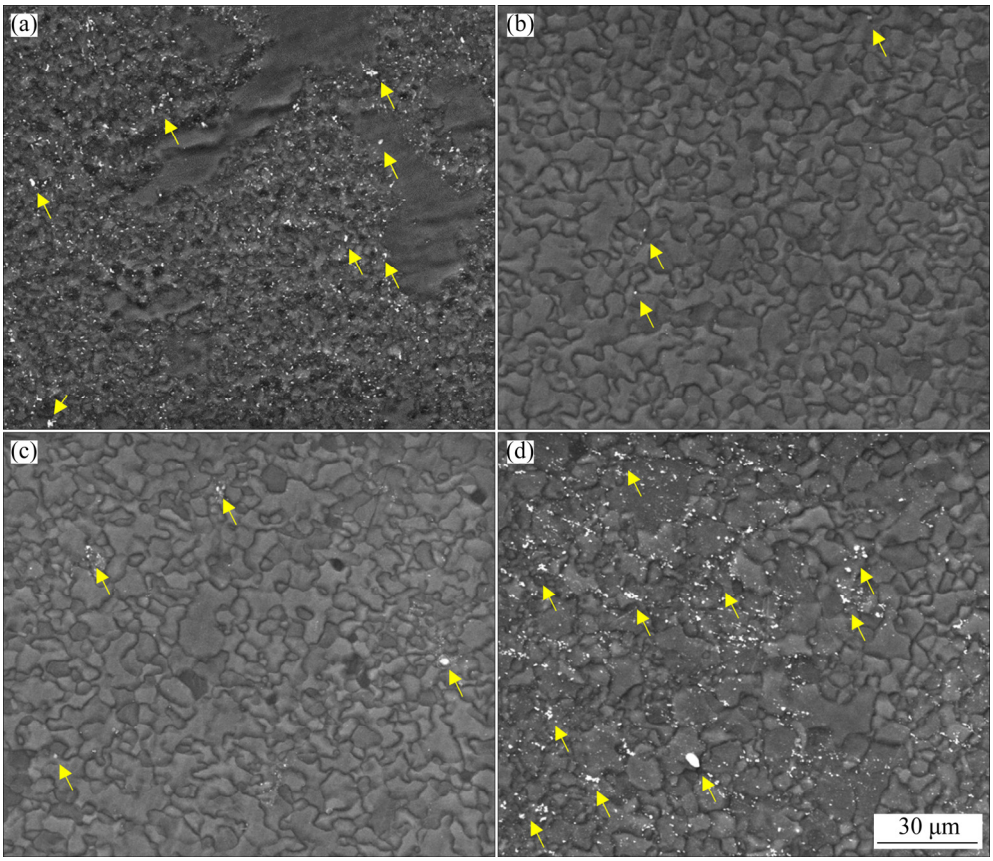

Fig. 5 SEM micrographs of AE (a), A1DE (b), A3DE (c), and A5DE (d) samples

growth of new strain-free grains occur in Mg alloys via various mechanisms such as continuous DRX (CDRX), discontinuous DRX (DDRX) or particle stimulated nucleation (PSN) depending on the alloy chemical composition and temperature, and mode of deformation [2,17,35]. The partial DRX in the AE sample can be attributed to the preferential nucleation on grain boundaries in the early deformation stage, and then it expands into grain through the evolution of sub-grain boundaries. It is in agreement with the results reported for extruded ZK60 alloy [36], and cast AM80 alloy [37] deformed at high temperatures. To confirm this phenomenon, optical images of the AE sample indicating more details in this specimen are shown in Fig. 4.

Fine and coarse grain size regions are visible in Figs. 4(a, b). Clearly, fine grains are located next to the boundaries of the elongated grains indicated by black arrows. Hence, it can be concluded that grain boundary nucleation followed by grain growth towards inside the elongated grains leads to the formation of a necklace structure after extrusion at 220 °C [17]. According to AL-SAMMAN et al [38], grain boundary bulging of new DRXed grains along initial grain boundaries or continuously via gradual transformation of subgrain boundaries into high angle boundaries is responsible for this type of microstructural evolution. Regarding A1DE, A3DE, and A5DE samples, the grain boundaries of DECLE processed specimens (Figs. 2(b−d)) act as the preferred nucleation sites for the formation of DRXed grains. Besides, a larger volume fraction of grain boundaries in the DECLEed samples resulted in the complete DRX and finer grain sizes of extruded sheets.

It has been proposed that second phase compounds are effective factors on the high-temperature strength and workability of Mg alloys [39]. According to the SEM results, fine second phase particles are distributed in the matrix of the AE sample (Fig. 5(a)), and their volume fraction is about 1.4%. According to our previous researches [9,40], the particles are mainly $MgZn_2$ and Mg_4Zn_7 [9]. Moreover, some Zr-containing particles were also detected by EDS in this sample, and their chemical composition (Fig. 6) is

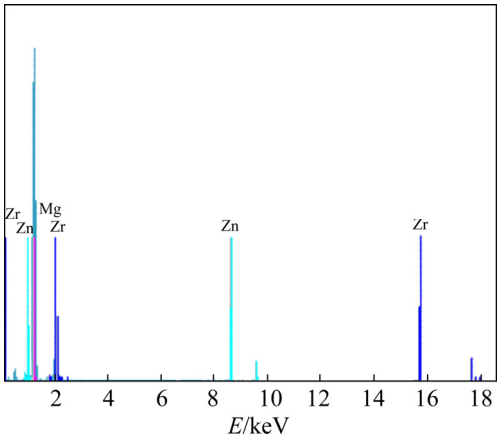

Fig. 6 EDS analysis result of Zr-rich second phase particles

$Mg_{88.2}Zr_{10.5}Zn_{1.3}$. FATEMI et al [41] proposed that Zr-rich particles caused crack initiation during deformation at temperatures of 225 and 300 °C, and reduced the workability of WE43 alloy [41]. It is clear in Figs. 5(b, c) that in the A1DE and A3DE samples, the volume fraction of second phase particles (indicated by yellow arrows) decreased to the amount of 0.3% and 0.5%, respectively. This can be explained by the dissolution of alloying elements inside the Mg matrix due to the larger volume fraction of grain boundaries that acted as the fast diffusion paths. Contrary to the A1DE and A3DE specimens, the volume fraction of second phase particles increased in the A5DE counterpart and reached to 2.6%. XRD analysis in our previous report suggested that the particles are $MgZn_2$ and MgZn in this sample [9]. It has been reported that in Mg−Zn system, the MgZn phase is thermo-dynamically stable and formed through deformation in high-temperature regimes. This phase formation can occur according to the sequence of $Mg_4Zn_7 \rightarrow MgZn_2 \rightarrow MgZn$ [42,43].

3.2 Flow behavior and constitutive model

SPT curves of the AE, A1DE, A3DE, and A5DE samples at temperatures of 200, 250, and 300 °C, and initial strain rates of 0.003−0.33 s^{-1} are illustrated in Figs. 7 and 8. It is obvious that the nature of these curves is similar to that of traditional tensile testing results, including a linear elastic part that deviated to a plastic deformation region at the yield point (SYS), and was followed by a work hardening part to reach the maximum point (USS). After the USS point, the strength continuously

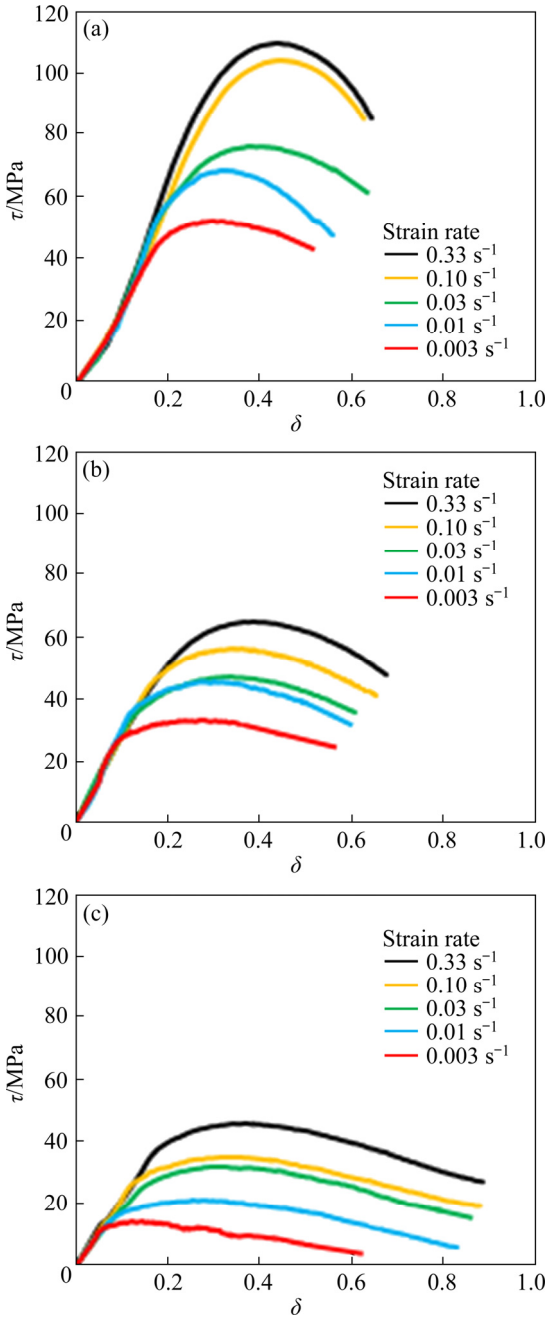

Fig. 7 SPT curves of AE sample at different shear strain rates and temperatures: (a) 200 °C; (b) 250 °C; (c) 300 °C

decreased until fracture happened. It can be seen in all of these curves that by increasing the temperature and decreasing the initial strain rate, the strength level of all samples was reduced. Besides, it is evident that at 300 °C, the post uniform region is near steady state in low strain rate conditions, which can be attributed to the equilibrium conditions between strain hardening and strain softening [22]. The strength reduction can be explained by easier dislocation movement at

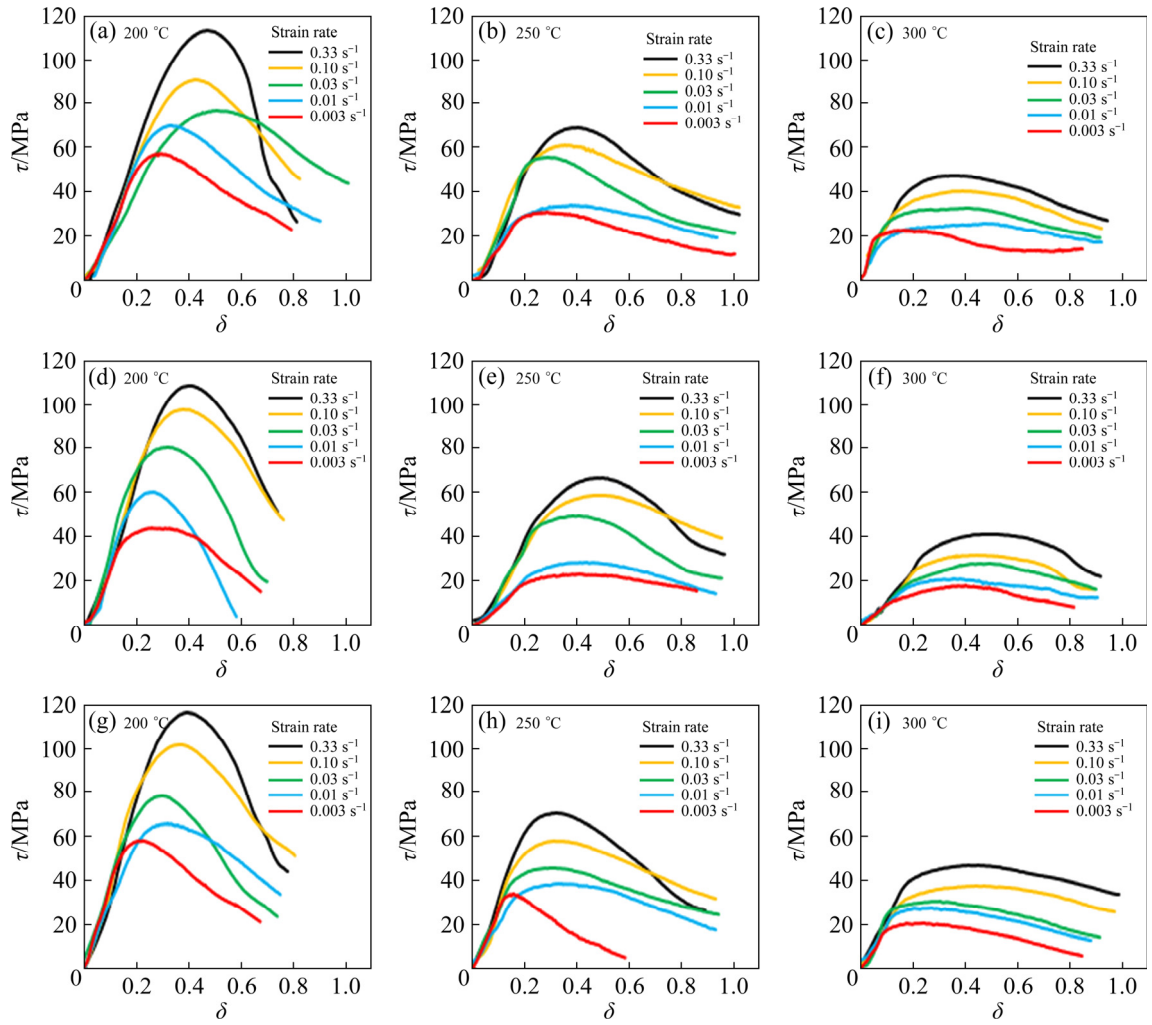

Fig. 8 SPT curves of DECLE samples at different temperatures and shear strain rates: (a−c) A1DE sample; (d−f) A3DE sample; (g−i) A5DE sample

higher temperatures due to the activation of non-basal slip systems, climbing and cross slip, and maybe due to annihilation and/or rearrangement of dislocations [22,44]. Similar results have been reported for other SPD-processed Mg alloys such as GZ31 [2], Mg−6Gd−3Y−0.5Ag [45], and Mg−2Gd [11]. The hardening phenomenon can be attributed to some microstructural evolutions such as dislocation formation and interaction [32,44]. The softening part occurred due to the dislocation rearrangement and/or annihilation caused by DRX at high temperatures [30,32,44]. It is worth mentioning that by increasing the temperature and decreasing the strain rate, the SPT curves reached the USS point at a smaller critical normalized displacement (δ).

The constitutive equations are attractive relationships among flow stress, temperature, and strain rate, and can be utilized to predict the flow behavior of materials in different practical situations for industrial applications. They are also used to construct computer simulations of flow behavior which aims at predicting flow curves under different deformation conditions. This broad applicability has triggered many research works to develop various types of constitutive equations [46]. As is mentioned earlier, the SPT curves (Figs. 7 and 8) could be used to develop a constitutive equation among shear stress (τ), shear strain rate ($\dot{\gamma}$), and temperature (T) [22,44]. The effect of strain rate and temperature on hot deformation can be expressed by the Zener−Hollomon parameter (Z) in an exponent type equation (Eq. (3)) [47]. On the other hand, the relationship among temperature, flow stress, and strain rate could be described by the Arrhenius type equation (Eqs. (4)−(6)) [48].

According to previous researches [22,44,49], it is reasonable to modify equations to a shear state by considering the von-Mises criterion $\sigma = \tau\sqrt{3}$ and $\varepsilon = \gamma\sqrt{3}$.

$$Z = \dot{\gamma}\exp[Q/(RT)] \tag{3}$$

$$\dot{\gamma} = A_1\tau^{n_1}\exp[-Q/(RT)] \tag{4}$$

$$\dot{\gamma} = A_2\exp(\beta\tau)\exp[-Q/(RT)] \tag{5}$$

$$\dot{\gamma} = A[\sinh(\alpha'\tau)]^n\exp[-Q/(RT)] \tag{6}$$

where $\dot{\gamma}$ is the shear strain rate, Q is the activation energy, T is the thermodynamic temperature, R is the molar gas constant (8.314 J/(mol·K)), τ is the shear flow stress, n, n_1, α, and β are material constants, and $\alpha'=\beta/n_1$. It has been reported from experimental results that n_1 in Eq. (4) is independent of temperature and is constant for the low stress regimes. Similarly, β in Eq. (5) is constant but at the higher stress ranges. According to the previous findings in the literature, it has been proven that Eq. (6) is able to make a better connection among $\dot{\gamma}$, τ, and T in a wide range of temperatures and strain rates [22,48,50]. Based on Taylor series expansion, at high stresses, $\sinh(\alpha'\tau)$ is almost equal to $\exp(\alpha'\tau)/2$ and Eq. (6) can be substituted by Eq. (5), with $A_2=2^nA\exp(-n_1)$. At low-stress levels, $\sinh(\alpha'\tau)$ is reduced to $(\alpha'\tau)$ and therefore Eq. (6) can be approximated by Eq. (4) with $A_1=A\alpha'^n$.

By taking the logarithm type of both sides, Eqs. (4)−(6) can be transformed into

$$\ln\dot{\gamma} = n_1\ln\tau + \ln A_1 - Q/(RT) \tag{7}$$

$$\ln\dot{\gamma} = \beta\tau + \ln A_2 - Q/(RT) \tag{8}$$

$$\ln\dot{\gamma} = n\ln[\sinh(\alpha'\tau)] + \ln A - Q/(RT) \tag{9}$$

Substituting the experimental values of τ and $\dot{\gamma}$ into the above equations, the material constants of n_1 and β could be obtained from the average slopes of every single line in the $\ln\dot{\gamma}-\ln\tau$ and $\ln\dot{\gamma}-\tau$ plots at a constant temperature by linear fit method, respectively. Thus, in this step, an approximate value of α' can be calculated.

Based on Eq. (9), the stress exponent, n, is determined from the average of the line slopes in $\ln\dot{\gamma}-\ln[\sinh(\alpha'\tau)]$ plots at different temperatures. The activation energy (Q) can be obtained by differentiating Eq. (9) with respect to $1/T$:

$$Q = Rn\left\{\frac{\partial\ln[\sinh(\alpha'\tau)]}{\partial(1/T)}\right\}_{\dot{\gamma}} \tag{10}$$

Combining Eq. (3) with Eq. (6) and taking natural logarithm give:

$$\ln Z = n\ln[\sinh(\alpha'\tau)] + \ln A \tag{11}$$

Finally, $\ln A$ can be estimated using the intercept of the linear relationship of $\ln Z-\ln[\sinh(\alpha'\tau)]$. Using the USS as τ and the shear strain rate as $\dot{\gamma}$, while using the described calculation sequence, the material constants of n, α', Q, and $\ln A$ have been obtained by curve fitting of plots such as Figs. 9 and 10 for AE and A5DE samples, respectively. The linear curves in Fig. 9 and Figs. 10(a, b) give the values of β' and n_1, respectively, and the value of α' is determined based on $\alpha'=\beta/n_1$. To assess the average sine hyperbolic stress exponent, n, the slopes of Figs. 9(c) and 10(c) were used for each condition of ZK60 alloy. All of the calculated n and α' values are shown in Table 3.

It is clear that the n values of 3.5−4.2 are obtained for all conditions, and α' is in the range of 0.021−0.025. The calculated n values are in the ranges that suggest dislocation creep as the predominant deformation mechanism in the temperature range of 200−300 °C in the extruded ZK60 alloy sheets [51]. Similar results have been reported for the shear deformation procedure of extruded Mg−3Gd−1Zn alloy in a temperature range of 300−500 °C [22]. By using Eq. (10) and Figs. 9(d) and 10(d), the mean amount of activation energy for hot shear deformation of all ZK60 samples can be obtained, as given in Table 3. Accordingly, the Q values are in the range of 125−139 kJ/mol, which is close to that of 135 kJ/mol for magnesium volume self-diffusion, indicating that the deformation of ZK60 alloy sheets is diffusion-controlled [26,51]. BARNETT [52] reported a Q value of 147 kJ/mol for an extruded AZ31 alloy. In addition, similar Q values are reported in other SPD-processed Mg alloys. For instance, ARUN and CHAKKINGAL [53] reported Q values in the range of 125−140 kJ/mol for AZ31 alloy deformed by different routes and passes of the ECAP method. Generally, according to the Q values close to 135 kJ/mol, dislocation creep in Mg alloys can be controlled by various mechanisms such as solute drag creep (n≈3.3) or dislocation climb (n≈5) [51]. Hence, considering the n and Q values in Table 3, it can be concluded that the main hot deformation mechanism for extruded ZK60 alloy sheets is dislocation creep controlled by dislocation climb and solute drag mechanism.

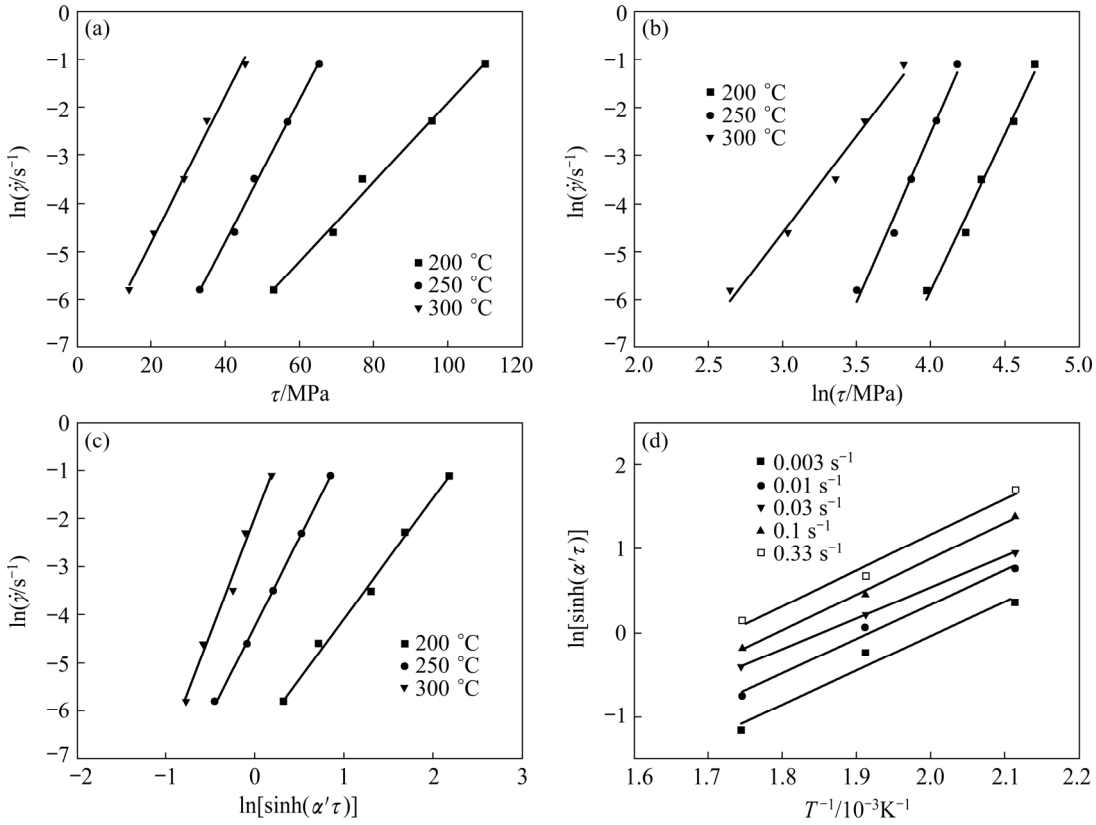

Fig. 9 Plots used for calculation of material constants for AE sample: (a) $\ln\dot{\gamma}-\tau$; (b) $\ln\dot{\gamma}-\ln\tau$; (c) $\ln\dot{\gamma}-\ln[\sinh(\alpha'\tau)]$; (d) $\ln[\sinh(\alpha'\tau)]-1/T$

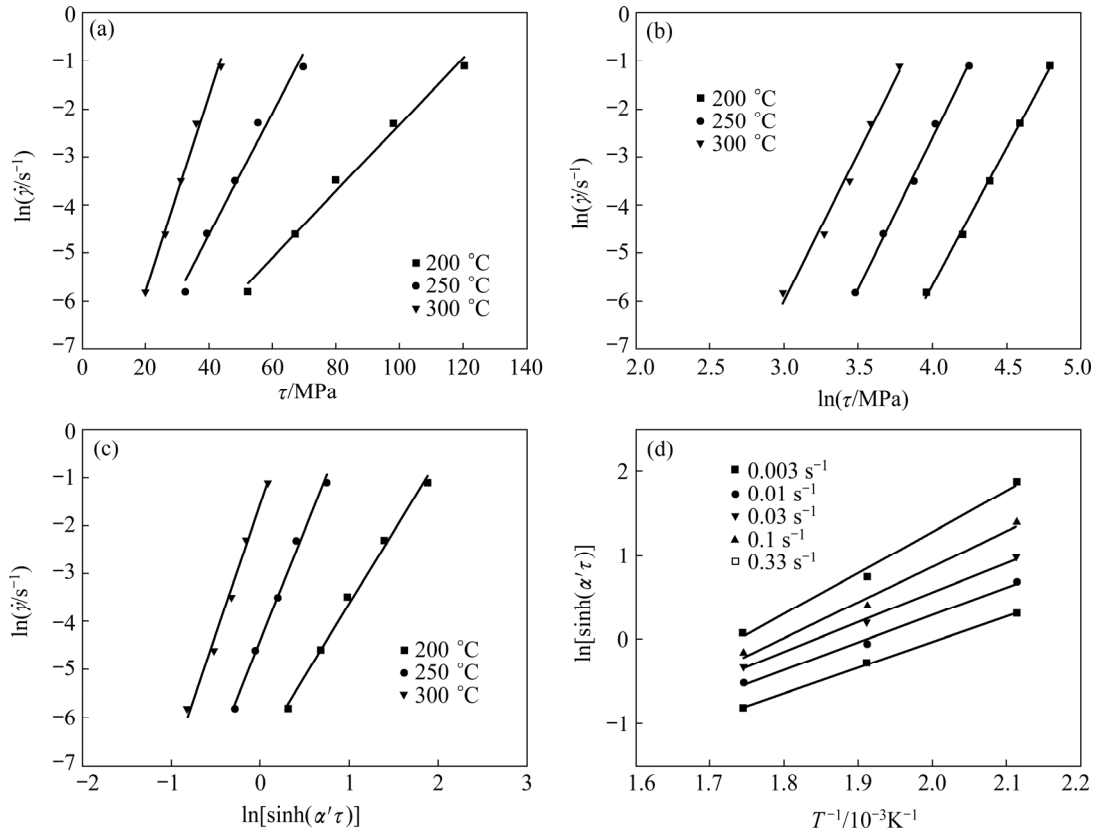

Fig. 10 Plots used for calculation of material constants for A5DE sample: (a) $\ln\dot{\gamma}-\tau$; (b) $\ln\dot{\gamma}-\ln\tau$; (c) $\ln\dot{\gamma}-\ln[\sinh(\alpha'\tau)]$; (d) $\ln[\sinh(\alpha'\tau)]-1/T$

Table 3 Microstructural features and n, α', Q, and ln A values for all processing conditions

Processing condition	Grain size/μm	Second phase particles content/%	n	α'	Q/(kJ·mol^{-1})	ln A'
AE	68	1.4	4.12	0.0218	139	27.6
A1DE	7.1	0.3	4.1	0.0221	137	26.93
A3DE	6	0.5	3.535	0.0249	125	24.24
A5DE	5.2	2.6	4.193	0.0214	130	25.33

It can be inferred from the results that while there is a significant grain refinement, and change in the secondary phase content, the mechanism of high-temperature deformation was not changed. This is indicated by the negligible differences between the stress−strain curves for all processed samples in Figs. 7 and 8, and also n and Q values in Table 3. It has been proposed that different parameters such as grain size, second phase particles, dislocation density, DRX volume fraction, and texture evolution affect the hot deformation behavior of Mg alloys, in other words, Q and n values [2,9]. Hence, the small difference among Q values in the present study can be explained by the microstructural characteristics shown in Table 3. As an example, the larger Q value of the AE sample in comparison to the A3DE specimen can be explained by the larger grain size (68 μm) and the greater volume fraction of second phase particles (1.4%) in the former sample in comparison to the latter one (grain size of 6 μm, second phase particles fraction of 0.5%). But, according to Table 3, it is clear that while the fraction of second phase particles is almost similar in A1DE and A3DE samples, the Q value was dropped in the latter sample which can be attributed to finer grain size (6.0 μm). Moreover, it can be seen that although the A5DE sample has a finer grain size compared to A3DE sample, the Q value of A5DE slightly increased compared to the A3DE. This can be deduced from higher second phase particles amount (2.6%) in this sample. Smaller n and Q values of the A3DE sample provide more significant formability in the temperature range of 200−300 °C in comparison to other samples.

It is well accepted that fine grain size reduces the activation energy for hot deformation of Mg alloys [2,9,53]. ARUN and CHAKKINGA [53] reported the decreasing of Q value in an AZ31B alloy due to the grain size reduction by applying ECAP passes. This could be ascribed to the presence of faster diffusion paths, i.e., grain boundaries, especially HAGBs, inside the microstructure. However, the large deformed un-DRXed grains, such as those present in the microstructure of the AE sample (Figs. 3(a) and 5(a)), can hinder the mobility of dislocations due to high density of dislocation networks [54] that interact with the moving dislocations at high temperatures, or the fact that non-equilibrium boundaries of the deformed grains induce long-range stresses and restrict dislocation motion during high-temperature deformation [55]. In addition, WANG et al [26] reported that the fine MgZn and $MgZn_2$ second phase particles, which are also detected in ZK60 alloy sheets in the present study (Fig. 5), can act as obstacles against dislocation movement during hot deformation of ZK60 alloy. It has been reported by MALIK et al [56] that the $MgZn_2$ particles are stable even at temperatures higher than 377 °C [56]. Moreover, HADADZADEH et al [39] reported that nano-sized particles in the Mg–5.4Zn–0.6Zr alloy lead to pinning of the migrating dislocations inside the un-DRXed grains.

As is obvious, although the mentioned microstructural characteristics affect the Q values, all of the ZK60 sheets still demonstrated almost similar n and Q values in the ranges of 3.5−4.2 and 125−139 kJ/mol, respectively, which indicate similar deformation mechanism. It also can be explained by textural evolution. Moreover, it is logically accepted that the basal slip is a predominant mechanism at low temperatures, while at higher temperatures, non-basal slip systems are activated during the plastic deformation [2,8]. According to our previous studies [9,40], all of the extruded ZK60 alloy sheets demonstrate a strong basal texture, i.e., the hexagonal c-axis of the HCP crystals is orientated parallel to the sheet surface normal direction (ND). The schematic illustration of the texture component of extruded sheets is shown in Fig. 11. This means that during SPT, the loading direction (Fig. 1) is parallel to the c-axis of each HCP crystal. As we proposed in our previous

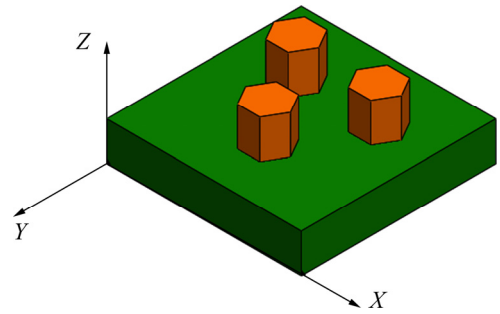

Fig. 11 Schematic illustration of predominant texture component of all extruded ZK60 alloy samples

research, in such a situation, slip in the basal (0001) and prismatic $(10\,\bar{1}0)$ planes are not easy because the stress is applied almost perpendicular to the $\langle 11\bar{2}0\rangle$ directions [40]. Similar results have been reported for the ZK60 alloy plate during compression loading parallel to ND where the (0001) and $(10\bar{1}0)$ planes were perpendicular and parallel to the compression axis, i.e., ND [31]. In this texture and loading configuration, it is expected that the second-order pyramidal slip system will be activated in the temperature range of 200−400 °C during SPT of the ZK60 alloy sheet [31]. BARNETT [52] suggested that the influence of texture on the flow stress of Mg alloys can persist even up to 450 °C. Accordingly, it can be concluded that in the present study the deformation mechanism, i.e., dislocation creep, competitively depends on microstructural characteristics; among them, basal texture in extruded ZK60 alloy sheets significantly controlled the deformation mechanism in the temperature range of 200−300 °C and resulted in similar n and Q values for all samples.

Figure 12 shows the variations of material constants (n and Q) with the grain size and second phase particles fraction (%) of ZK60 Mg alloy obtained under different conditions. To predict the material constant values within the range of our data, a surface was fitted to n and Q variations. It can be seen that decreasing the grain size to <10 μm and also the presence of near 1% second phase fraction leads to the least n and Q values and the superplastic properties (n≈2) are expected to be observed in these regions. One of the most important factors to achieve superplastic behavior in Mg alloys is the grain size stability during high-temperature deformation [2]. This stability can be obtained when second phase particles are present at the grain boundaries and forbid their migration. Hence, in the cases that second phase particles are scant, about 0.5% in Fig. 12(a), the microstructure is susceptible to grain growth during hot deformation followed by a large amount of n (≈4). When a large amount of second phase particles exists in the microstructure, cracking around them is a possible phenomenon [40] that restricts high amounts of formability and consequently higher values of n are achieved (Fig. 12(a)).

After evaluating material constants for each sample, a constitutive equation can be developed to predict the peak shear flow stress. With the definition of the Zener−Hollomon parameter, Z (Eq. (3)), and by solving Eq. (11), the peak shear flow stress can be written as a function of the Z parameter as shown below:

$$\tau=\frac{1}{\alpha'}\ln\left\{\left(Z/A'\right)^{1/n}+\left(1+\left(Z/A'\right)^{2/n}\right)^{0.5}\right\} \tag{12}$$

Table 4 shows all the equations used for the prediction of shear flow stress at various temperatures and shear strain rates derived for

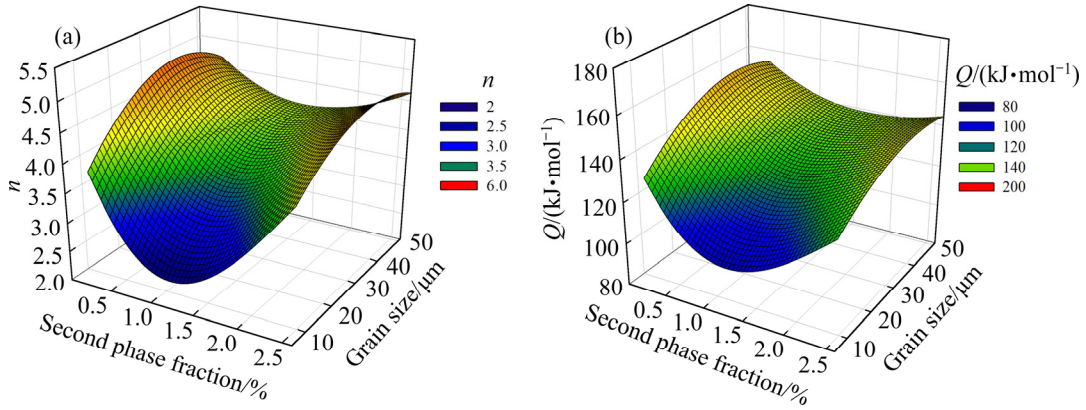

Fig. 12 Variation of material parameters, n (a) and Q (b), with second phase fraction and grain size for ZK60 Mg alloy

Table 4 Constitutive equations developed for prediction of peak shear flow stress for different processing conditions

Processing condition	Peak shear flow stress equation
AE	$\tau = 45.82\ln\{(Z/A')^{0.2427} + [(Z/A')^{0.4854} + 1]^{1/2}\}$
A1DE	$\tau = 45.17\ln\{(Z/A')^{0.2439} + [(Z/A')^{0.4878} + 1]^{1/2}\}$
A3DE	$\tau = 40.07\ln\{(Z/A')^{0.2829} + [(Z/A')^{0.5659} + 1]^{1/2}\}$
A5DE	$\tau = 46.62\ln\{(Z/A')^{0.2385} + [(Z/A')^{0.4770} + 1]^{1/2}\}$

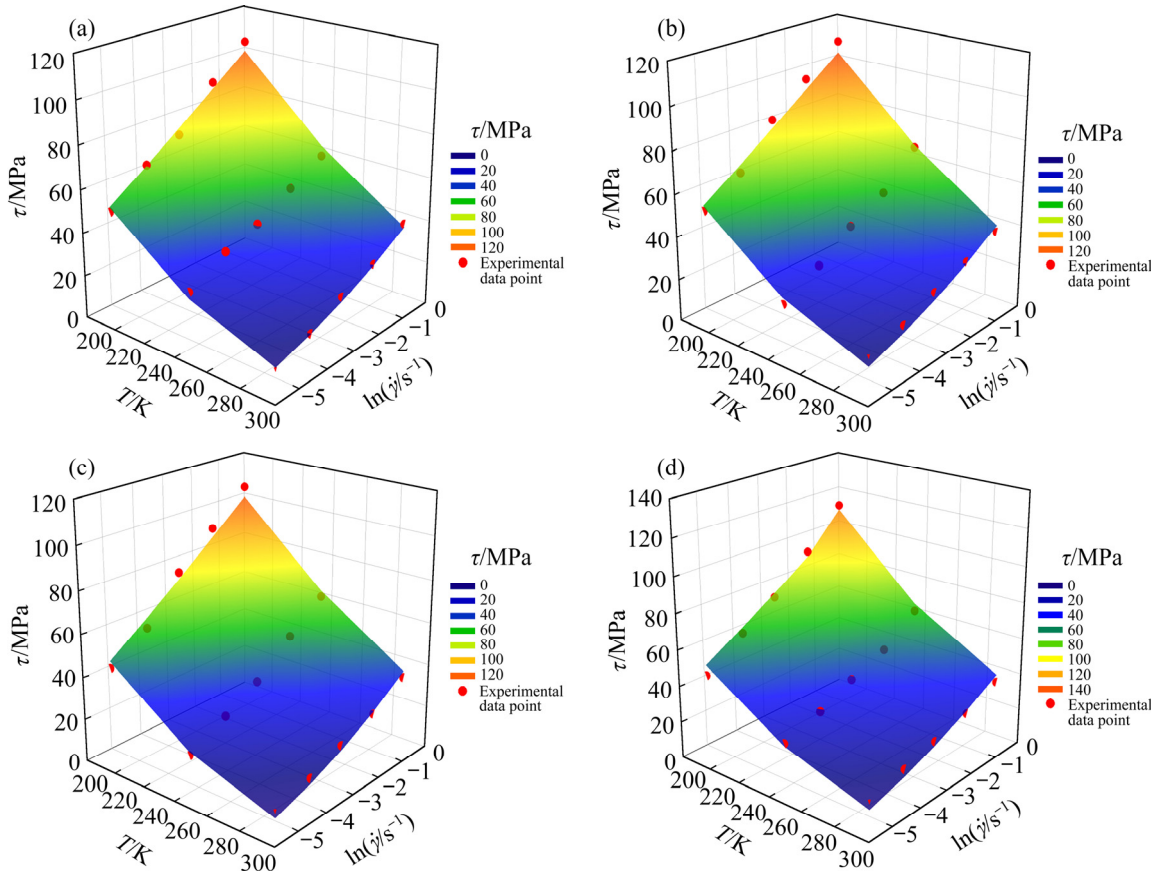

Fig. 13 Correlation of predicted and experimental shear flow stress of ZK60 Mg alloy for different conditions: (a) AE; (b) A1DE; (c) A3DE; (d) A5DE

annealed and DECLEed specimens. The derived equations presented in Table 4 were validated to predict shear flow stress. Hence, the predicted shear flow stresses were plotted as surfaces, while experimental shear flow stresses were shown by points in Fig. 13. As can be seen in this figure, the conformity between the maximum shear stresses predicted by equations and those of experiments is desirable, and the R^2 values for the constitutive models are over 0.98 for all conditions.

4 Conclusions

(1) The fine grain and homogeneous microstructure with the average grain size of 6.0 and 5.2 μm after 3 and 5 passes of DECLE and following extrusion could be obtained, respectively. These fine-grained microstructures compared to the coarse grain structure obtained after the sheet extrusion of annealed sample (68 μm), prove that initial microstructure before sheet extrusion could have a drastic influence on the microstructure of sheets.

(2) SPT results were successfully used to develop constitutive equations. The predicted shear flow stresses using the equations are in good agreement with the experimentally determined peak shear flow stress values.

(3) By investigating ZK60 Mg alloy with a different history of forming, it was concluded that material constants of n and Q are dependent on the microstructure parameters such as grain size and

second phase particle fractions and textural evolution.

(4) The relationship of n and Q with grain size and second phase particle fractions was anticipated using a 3D surface and their variations were investigated. It was concluded that the presence of 1 vol.% second phase particles and also grain sizes lower than 10 μm is essential to achieve suitable low n and Q values for superplastic forming.

(5) The smallest n and Q values were obtained for the A3DE sample with the grain size of 6.0 μm and presence of 0.5% second phase particles.

References

[1] HADADZADEH A, WELLS M A, SHAHA S K, JAHED H, WILLIAMS B W. Role of compression direction on recrystallization behavior and texture evolution during hot deformation of extruded ZK60 magnesium alloy [J]. Journal of Alloys and Compounds, 2017, 702: 274−289.

[2] SABBAGHIAN M, MAHMUDI R. Superplasticity of the fine-grained friction stir processed Mg–3Gd–1Zn sheets [J]. Materials Characterization, 2021, 172: 110902.

[3] DAI S, WANG F, WANG Z, LIU Z, MAO P L. Effect of Cu on microstructure, mechanical properties, and texture evolution of ZK60 alloy fabricated by hot extrusion−shearing process [J]. Transactions of Nonferrous Metals Society of China, 2020, 30(6): 1511−1523.

[4] SABBAGHIAN M, MAHMUDI R. Microstructural evolution and local mechanical properties of friction stir processed Mg−3Gd−1Zn cast Alloy [J]. Journal of Materials Engineering and Performance, 2016, 25: 1856−1863.

[5] SIAHSARANI A, FARAJI G. Processing and characterization of AZ91 magnesium alloys via a novel severe plastic deformation method: Hydrostatic cyclic extrusion compression (HCEC) [J]. Transactions of Nonferrous Metals Society of China, 2021, 31(5): 1303−1321.

[6] SONG B, DU Z W, YANG Q S, GUO N, GUO S F, YU J C, XIN R L. Effect of pre-rolling path on mechanical properties of rolled ZK60 alloys [J]. Transactions of Nonferrous Metals Society of China, 2021, 31(5): 1322−1338.

[7] SABBAGHIAN M, MAHMUDI R, SHIN K S. Effect of texture and twinning on mechanical properties and corrosion behavior of an extruded biodegradable Mg−4Zn alloy [J]. Journal of Magnesium and Alloys, 2019, 7(4): 707−716.

[8] WANG W K, CHEN W Z, ZHANG W C, CUI G R, WANG E D. Weakened anisotropy of mechanical properties in rolled ZK60 magnesium alloy sheets with elevated deformation temperature [J]. Journal of Materials Science & Technology, 2018, 34(11): 2042−2050.

[9] FAKHAR N, SABBAGHIAN M, NAGY P, FEKETE K, GUBICZA J. Superior low-temperature superplasticity in fine-grained ZK60 Mg alloy sheet produced by a combination of repeated upsetting process and sheet extrusion [J]. Materials Science and Engineering A, 2021, 819: 141444.

[10] MILIND T R, DATE P P. Analytical and finite element modeling of strain generated in equal channel angular extrusion [J]. International Journal of Mechanical Sciences, 2012, 56(1): 26−34.

[11] AZIZI N, MAHMUDI R. Superplasticity of fine-grained Mg–xGd alloys processed by multi-directional forging [J]. Materials Science and Engineering A, 2019, 767: 138436.

[12] HOSEINI-ATHAR M M, MAHMUDI R, REVATHY RAJAN P B, HEDSTRÖM P. Microstructure and superplasticity of Mg–2Gd–xZn alloys processed by equal channel angular pressing [J]. Materials Science and Engineering A, 2021, 808: 140921.

[13] CUI C, ZHANG W C, CHEN W Z, HE J, CHEN X M, HOU J B. Microstructure, texture evolution and yield strength symmetry improvement of as-extruded ZK60 Mg alloy via multi-directional impact forging [J]. Journal of Magnesium and Alloys, 2021.

[14] GUO W, WANG Q D, YE B, LIU M P, PENG T, LIU X T, ZHOU H. Enhanced microstructure homogeneity and mechanical properties of AZ31 magnesium alloy by repetitive upsetting [J]. Materials Science and Engineering A, 2012, 540: 115−122.

[15] FAKHAR N, FERESHTEH-SANIEE F, MAHMUDI R. Significant improvements in mechanical properties of AA5083 aluminum alloy using dual equal channel lateral extrusion [J]. Transactions of Nonferrous Metals Society of China, 2016, 26(12): 3081−3090.

[16] FERESHTEH-SANIEE F, FAKHAR N, KARAMI F, MAHMUDI R. Superior ductility and strength enhancement of ZK60 magnesium sheets processed by a combination of repeated upsetting and forward extrusion [J]. Materials Science and Engineering A, 2016, 673: 450−457.

[17] PRAKASH P, TOSCANO D, SHAHA S K, WELLS M A, JAHED H, WILLIAMS B W. Effect of temperature on the hot deformation behavior of AZ80 magnesium alloy [J]. Materials Science and Engineering A, 2020, 794: 139923.

[18] FAKHAR N, KHADEMI E, MOMENI A. High temperature behavior of severely deformed AA 5083 through equal channel lateral extrusion [J]. Materials Chemistry and Physics, 2020, 243: 122581.

[19] HUANG W Y, YANG X Y, YANG Y, MUKAI T, SAKAI T. Effect of yttrium addition on the hot deformation behaviors and microstructure development of magnesium alloy [J]. Journal of Alloys and Compounds, 2019, 786: 118−125.

[20] GUDURU R K, DARLING K A, KISHORE R, SCATTERGOOD R O, KOCH C C, MURTY K L. Evaluation of mechanical properties using shear–punch testing [J]. Materials Science and Engineering A, 2005, 395(1/2): 307−314.

[21] HOSEINI-ATHAR M M, MAHMUDI R, PRASATH BABU R, HEDSTRÖM P. Effect of Zn addition on dynamic recrystallization behavior of Mg−2Gd alloy during high-temperature deformation [J]. Journal of Alloys and Compounds, 2019, 806: 1200−1206.

[22] SAREBANZADEH M, MAHMUDI R, ROUMINA R. Constitutive analysis and processing map of an extruded Mg–3Gd–1Zn alloy under hot shear deformation [J]. Materials Science and Engineering A, 2015, 637: 155−161.

[23] ALIZADEH R, MAHMUDI R, RUANO O A, NGAN A H W. Constitutive analysis and hot deformation behavior of fine-grained Mg−Gd−Y−Zr alloys [J]. Metallurgical and Materials Transactions A, 2017, 48: 1−11.

[24] YANG Q, FENG A H, XIAO B L, MA Z Y. Influence of texture on superplastic behavior of friction stir processed ZK60 magnesium alloy [J]. Materials Science and Engineering A, 2012, 556: 671−677.

[25] FAKHAR N, SABBAGHIAN M. A good combination of ductility, strength, and corrosion resistance of fine-grained ZK60 magnesium alloy produced by repeated upsetting process for biodegradable applications [J]. Journal of Alloys and Compounds, 2021, 862: 158334.

[26] WANG S Y, GAO L, LUO A, LI D J, ZENG X Q. Hot deformation behavior and workability of pre-extruded ZK60A magnesium alloy [J]. Transactions of Nonferrous Metals Society of China, 2015, 25(6): 1822−1830.

[27] FIGUEIREDO R B, LANGDON T G. The development of superplastic ductilities and microstructural homogeneity in a Magnesium ZK60 alloy processed by ECAP [J]. Materials Science and Engineering A, 2006, 430(1/2): 151−156.

[28] LI J Q, LIU J, CUI Z S. Characterization of hot deformation behavior of extruded ZK60 magnesium alloy using 3D processing maps [J]. Materials & Design, 2014, 56: 889−897.

[29] YU Y D, KUANG S Z, CHU D S, ZHOU H, LI J, LI C X. Microstructure and low-temperature superplasticity of fine-grain ZK60 magnesium alloy produced by equal-channel angular pressing [J]. Metallography, Microstructure, and Analysis, 2015, 4: 518−524.

[30] HADADZADEH A, WELLS M A. Analysis of the hot deformation of ZK60 magnesium alloy [J]. Journal of Magnesium and Alloys, 2017, 5(4): 369−387.

[31] CHALASANI D, RAO K P, JAIN M K, PRASAD Y V R K. Role of loading direction on compressive deformation behavior of extruded ZK60 alloy plate in a wide range of temperature [J]. Journal of Alloys and Compounds, 2018, 744: 289−300.

[32] CHENG Q, CHEN L, TANG J W, ZHAO G Q, SUN L, ZHANG C S. A comprehensive analysis on microstructure evolution of Mg−5.65Zn−0.66Zr alloy during hot deformation [J]. Journal of Magnesium and Alloys, 2021, 9(2): 520−531.

[33] CABRERA J, DUMITRU F D, HIGUERA COBOS O. ZK60 alloy processed by ECAP: Microstructural, physical and mechanical characterization [J]. Materials Science and Engineering A, 2014, 594: 32−39.

[34] LI X, JIANG J H, ZHAO Y H, MA A B, WEN D J, ZHU Y T. Effect of equal-channel angular pressing and aging on corrosion behavior of ZK60 Mg alloy [J]. Transactions of Nonferrous Metals Society of China, 2015, 25(12): 3909−3920.

[35] GALIYEV A, KAIBYSHEV R, GOTTSTEIN G. Correlation of plastic deformation and dynamic recrystallization in magnesium alloy ZK60 [J]. Acta Materialia, 2001, 49: 1199−1207.

[36] KIM B, KIM J C, LEE S, LEE K S, LEE J G, PARK S S. High-strain-rate superplasticity of fine-grained Mg–6Zn–0.5Zr alloy subjected to low-temperature indirect extrusion [J]. Scripta Materialia, 2017, 141: 138−142.

[37] GUO P C, LIU X, ZHU B W, LIU W H, ZHANG L Q. The microstructure evolution and deformation mechanism in a casting AM80 magnesium alloy under ultra-high strain rate loading [J]. Journal of Magnesium and Alloys, 2021. Doi: 10.1016/j.jma.2021.07.032.

[38] AL-SAMMAN T, LI X, GHOSH CHOWDHURY S. Orientation dependent slip and twinning during compression and tension of strongly textured magnesium AZ31 alloy [J]. Materials Science and Engineering A, 2010, 527: 3450−3463.

[39] HADADZADEH A, MOKDAD F, AMIRKHIZ B S, WELLS M, WILLIAMS B W, CHEN D L. Bimodal grain microstructure development during hot compression of a cast-homogenized Mg−Zn−Zr alloy [J]. Materials Science and Engineering A, 2018, 724: 421−430.

[40] SABBAGHIAN M, FAKHAR N, NAGY P, FEKETE K, GUBICZA J. Investigation of shear and tensile mechanical properties of ZK60 Mg alloy sheet processed by rolling and sheet extrusion [J]. Materials Science and Engineering A, 2021, 828: 142098.

[41] FATEMI S M, ALIYARI S, MIRESMAEILI S M. Dynamic precipitation and dynamic recrystallization during hot deformation of a solutionized WE43 magnesium alloy [J]. Materials Science and Engineering A, 2019, 762: 138076.

[42] GAO X, NIE J F. Structure and thermal stability of primary intermetallic particles in an Mg–Zn casting alloy [J]. Scripta Materialia, 2007, 57: 655−658.

[43] NIE J F. Precipitation and hardening in magnesium alloys [J]. Metallurgical and Materials Transactions A, 2012, 43: 3891−3939.

[44] BAYAT TORK N, MAHMUDI R, HOSEINI-ATHAR M M. Hot deformation constitutive analysis and processing maps of extruded Mg–Gd binary alloys [J]. Journal of Materials Research and Technology, 2020, 9(6): 15346−15359.

[45] REZAEI A, MAHMUDI R, CAYRON C, LOGE R E. Superplastic behavior of a severely deformed Mg–6Gd−3Y−0.5Ag alloy [J]. Materials Science and Engineering A, 2021, 802: 140616.

[46] LIN Y C, CHEN X M. A critical review of experimental results and constitutive descriptions for metals and alloys in hot working [J]. Materials & Design, 2011, 32(4): 1733−1759.

[47] ZENER C, HOLLOMON J H. Effect of strain rate upon plastic flow of steel [J]. Journal of Applied Physics, 1944, 15(1): 22−32.

[48] SHANG X, CUI Z, FU M W. A ductile fracture model considering stress state and Zener–Hollomon parameter for hot deformation of metallic materials [J]. International Journal of Mechanical Sciences, 2018, 144: 800−812.

[49] HOSEINI-ATHAR M M, MAHMUDI R. Effect of Zn content on hot deformation behavior of extruded Mg–Gd–Zn alloys [J]. Materials Science and Engineering A, 2019, 759: 745−753.

[50] SELLARS C M, MCTEGART W J. On the mechanism of hot deformation [J]. Acta Metallurgica, 1966, 14: 1136−1138.

[51] SOMEKAWA H, HIRAI K, WATANABE H, TAKIGAWA Y, HIGASHI K. Dislocation creep behavior in Mg−Al−Zn

alloys [J]. Materials Science and Engineering A, 2005, 407: 53−61.
[52] BARNETT M. Influence of deformation conditions and texture on the high temperature flow stress of magnesium AZ31 [J]. Journal of Light Metals, 2001, 1(3): 167−177.
[53] ARUN M S, CHAKKINGAL U. A constitutive model to describe high temperature flow behavior of AZ31B magnesium alloy processed by equal-channel angular pressing [J]. Materials Science and Engineering A, 2019, 754: 659−673.
[54] SABBAGHIAN M, MAHMUDI R, SHIN K S. Microstructural evolution, mechanical properties, and biodegradability of a Gd-containing Mg−Zn alloy [J]. Metallurgical and Materials Transactions A, 2021, 52: 1269−1281.
[55] MOHAMMAD F, PANIGRAHI S. Achieving excellent superplasticity in an ultrafine-grained QE22 alloy at both high strain rate and low-temperature regimes [J]. Journal of Alloys and Compounds, 2018, 747: 71−82.
[56] MALIK A, WANG Y, CHENG H, BHATTI T, NAZEER F. Superplastic behavior of fine-grained extruded ZK61 Mg alloy [J]. Results in Physics, 202, 20: 103731.

等通道侧向挤压和板材挤压法制备细晶 ZK60 镁合金板材的热剪切变形本构分析

N. FAKHAR[1], M. SABBAGHIAN[2]

1. Mechanical Engineering Department, Hamedan University of Technology, Hamedan, Iran;
2. School of Metallurgical and Materials Engineering, College of Engineering, University of Tehran, Tehran, Iran

摘　要：采用不同道次等通道侧向挤压(DECLE)和板材挤压成形发制备细晶 ZK60 合金板材。经过 3 和 5 道次 DECLE 和后续挤压后，退火样品中的粗大晶粒(68 μm)分别变为 6.0 μm 和 5.2 μm 的细小晶粒。基于冲孔剪切实验(SPT)结果建立本构方程，研究合金的热剪切变形行为。SPT 的温度范围为 200~300 ℃，应变率范围为 0.003~0.33 s^{-1}。计算结果表明，所有条件下制备的样品的活化能为 125~139 kJ/mol，应力指数为 3.5~4.2，表明主要的热变形机制是位错蠕变，由位错攀移和溶质拖曳机制控制。材料常数 n 和 Q 取决于晶粒尺寸，第二相颗粒比例等微观结构因素，通过三维曲面曲线预测了二者的关系。此外，挤压后的 ZK60 板材具有相似的强基面织构，因此，合金在 SPT 过程中具有相同的变形机制与相近的 n 和 Q 值。

关键词：ZK60 镁合金；本构方程；挤压；热变形；冲孔剪切实验；金属成型

(Edited by Bing YANG)